SEIS MICA

Imaging the Western Edge of the Aegean Shear Zone: The South Evia 2022-2023 Seismic Sequence

Christos P. Evangelidis [ID] [*][1] **, Ioannis Fountoulakis** [ID] [1,2]

[1]Institute of Geodynamics, National Observatory of Athens, Athens, Greece, [2]Department of Geology, University of Patras, Patras, Greece

Author contributions: *Conceptualization*: C.P.Evangelidis. *Methodology*: I.Fountoulakis. *Software*: I.Fountoulakis. *Formal Analysis*: I.Fountoulakis, C.P.Evangelidis. *Writing - original draft*: C.P.Evangelidis. *Writing - Review & Editing*: C.P.Evangelidis,I.Fountoulakis. *Visualization*: C.P.Evangelidis. *Supervision*: C.P.Evangelidis.

Abstract   This report presents the 2022-2023 South Evia island seismic sequence, in the western Aegean sea. An automated workflow, undergoing testing for efficient observatory monitoring in the wake of dense aftershock sequences, was employed to enhance the seismic catalog. It includes a deep-learning phase picker, absolute and relative hypocenter relocation, and moment tensor automatic calculations. The relocated catalog reveals a concentration of earthquake epicenters in a narrow NW-SE zone, with sinistral strike-slip fault movement. The findings of the study indicate the occurrence of an asymmetric rupture within conjugate fault structures in the western Aegean region. These fault structures, although not necessarily both active, play a significant role in marking the transition from dextral (SW-NE) to sinistral (NW-SE) strike-slip ruptures, connecting the Aegean shear zone with normal faulting in mainland Greece. The South Evia 2022-2023 seismic sequence has revealed the activation of this NW-SE strike-slip structure, contrary to previous assumptions of low seismicity in the region. The study highlights the importance of reassessing seismic hazard maps and considering the potential activation of similar zones further south in the future. It also emphasizes the need for the expansion and the densification of seismic networks within the Aegean.

Non-technical summary   This report presents a study on the seismic activity that occurred in the South Evia island region of the western Aegean Sea from 2022 to 2023. In order to analyze the earthquake data, a range of advanced automatic techniques, including state-of-the-art machine learning methods, were employed and tested for rapid observatory monitoring after significant aftershock sequences. The study's findings show that earthquake epicenters are concentrated in a narrow zone running from northwest to southeast. The movement along these faults suggests a horizontal left-lateral strike-slip motion. Asymmetric rupture occurring within interconnected fault structures in the western Aegean region plays a significant role in the transition from right-lateral strike-slip fault motion (southwest to northeast) to left-lateral strike-slip (northwest to southeast). The South Evia 2022-2023 seismic sequence shows the activation of a fault structure with northwest-to-southeast strike-slip horizontal motion, contradicting previous assumptions of low seismicity in the area. The study emphasizes the need to reevaluate seismic hazard maps in the region and consider the possibility of similar fault zones being activated further south in the future. It also emphasizes the need to expand the coverage of the seismic networks in the Aegean.

Introduction

The occurrence of two moderate events on the eastern shores of Evia Island in central Greece on November 29, 2022 (moment magnitude (Mw) 4.6 04:32 UTC and Mw 4.8 20:06 UTC), resulted in unrest among the civilian population in the Athens metropolitan area, situated around 50 km to the east. A series of minor preshocks was initiated a month before. The moment tensors (MTs) for the mainshocks provided by the National Observatory of Athens (NOA) revealed strike-slip focal mechanisms with either NW-SE or SW-NE strikes. As of June 2023, microearthquake activity persists, including an event of Mw 4.5 that took place on April 22, 2023.

The northern and central parts of the Aegean Sea are dominated by strike-slip zones that reflect the east-ward shear transmitted from major and minor branches of the North Anatolian Fault (NAT) (e.g. Barbot and Weiss, 2021). These right-lateral strike-slip zones continue westward and end near the primarily E-W oriented normal faulting system, which governs the Greek mainland. It seems that the strike-slip faulting extends as far as Evia Island, but it does not traverse through central Greece (Fig.1). To date, no active faults on the surface have been identified in the southern part of Evia Island (Ganas et al., 2013). Moreover, the Greek Database of Seismogenic Sources (GreDaSS) does not report the existence of seismogenic faults in this area (Caputo and Pavlides, 2013). According to the routine seismic catalogs provided by NOA, the studied region exhibits relatively limited background seismicity compared to other areas in Greece. As a result, this region has been considered to have relatively lower seismic

*Corresponding author: cevan@noa.gr

hazard compared to other regions of mainland Greece (Danciu et al., 2021).

In this report, we image the earthquake activity in the area by utilizing automated techniques to significantly enhance the NOA seismic catalog and image the details of the ruptured faults. We produce a new seismic catalog by deploying a deep-learning phase picker (Mousavi et al., 2020), a rapid arrival earthquake association (Zhang et al., 2019), an absolute location (Klein, 2002), and a relative relocation method (Trugman and Shearer, 2017). We also calculate as many as possible MTs solutions using *Gisola,* an automated regional moment tensor determination tool (Triantafyllis et al., 2021). This seismic monitoring workflow was first implemented by Fountoulakis et al. (2023), after the Mw 7.0 earthquake that occurred in Samos in 2020. Our primary objective is to establish this procedure as an operational system at NOA for analyzing dense aftershock sequences captured by numerous permanent and temporary seismic stations.

Event detection and location

Continuous seismic records from broadband seismic stations located up to 110 km from the main events epicenters were used for the period between October 2022 and April 2023 (Fig. 1). The installation of additional stations from the temporary network 1Y (Wolfgang Friederich et al., 2022), part of the AdriaArray experiment, improved significantly the seismic monitoring capacity in the area.

Using the EQTransformer signal detector (Mousavi et al., 2020), a deep-learning-based system that uses an attention mechanism to detect seismic signals and identify primary and secondary seismic arrivals, we identify earthquake signals and pick P and S seismic wave onsets. The independently identified arrivals are associated with seismic events using the REAL associator and initial locator (Zhang et al., 2019). It deploys a 3D grid around the station with the first recorded P arrival and searches for possible earthquake locations by counting other seismic arrivals within a time window based on theoretical traveltimes. To assure high-quality events, we required event identification with at least *four* P and S phases each. The local P-wave velocity model by Konstantinou et al. (2020) with V_p/V_s=1.73 was employed for the theoretical traveltime calculations.

We locate the associated events with the HYPOINVERSE code (Klein, 2002). Low-quality events with azimuthal gaps > 280°, average root-mean-square (RMS) residuals > 0.5 sec, and horizontal/vertical error > 0.5 km were discarded from the catalog, leaving 5838 well-located events. We further improve the earthquake locations using the GrowClust code (Trugman and Shearer, 2017), which incorporates techniques for hierarchical clustering and relocation based on waveform cross-correlation (WCC) values. We cross-correlate waveforms for event pairs that appear in common stations. To ensure high relocation precision, we consider only event pairs with 0.65 average minimum WCC values and a minimum of three phases with WCC values > 0.65. From the 5838 events in the input catalog, 1893

events were successfully relocated and clustered. The exclusive utilization of WCC relocation was driven by the objective of focusing specifically on events that were effectively located. This deliberate choice enabled the precise mapping of the activated fault structures within the designated study area, as depicted in Fig. 2. Growclust utilizes the bootstrap method to assess formal uncertainties by resampling the input WCC data. This iterative process generates a perturbed set of event locations that is specific to each bootstrap iteration. To calculate the relative relocation uncertainties, bootstrapping was employed with 30 resamplings of the input WCC data, resulting in mean horizontal and vertical errors of approximately 500 m and 450 m, respectively. For the detected and relocated final catalogs, the local magnitudes (M_L) were calculated using the local magnitude scale of Scordilis et al. (2016).

To precisely pinpoint the hypocenters of the three greatest events, we relied mostly on the manual seismic phases provided by NOA and the NonLinLoc location code (Lomax et al., 2000). Here, we do not perform GrowClust relocation because the waveforms from these larger events do not correlate well with those from the other smaller events. NonLinLoc was chosen due to its ability to account for the non-linear nature of the problem, allowing for a solid uncertainty analysis and providing a probability density function, resulting in a more comprehensive representation of the error volume. Hypocenter solutions of these events are presented in Table S1.

The magnitude characteristics of the catalog were additionally examined by analyzing the Frequency-Magnitude distribution. To estimate the magnitude of completeness (Mc) and the corresponding b-values, we employed the Maximum Curvature method proposed by Wiemer and Wyss (2000). As shown in Figure 3 and Table S2, there is a reduction of Mc for the WCC catalog (Mc 1.4) compared to the manually compiled institutional NOA catalog (Mc 1.8) and a significant increase in the detectability levels just by employing automated signal detector and associator routines without WCC (Mc 0.9).

Moment tensor (MT) solutions for the major events of the sequence were obtained using Gisola (Triantafyllis et al., 2021). Table S3 lists those events with reliable solutions.

Results and Discussion

The relocated catalog reveals a concentration of epicenters aligned in a narrow NW-SE zone, spanning approximately 5 to 6 kilometers in length (Fig. 2a). This alignment corresponds to the predominant NW-trending sinistral strike-slip fault plane in most calculated MTs, oriented approximately $130°$N. When examining a vertical cross-section along the strike, it becomes evident that the majority of events are clustered offshore, specifically within a 3 km long segment (Fig. 2b). Most of these events are confined between 8 to 12 km depth (Fig. 2b). Additionally, a lateral migration of events is observed, originating from the foreshocks (Figure S1). This migration, at an approximate
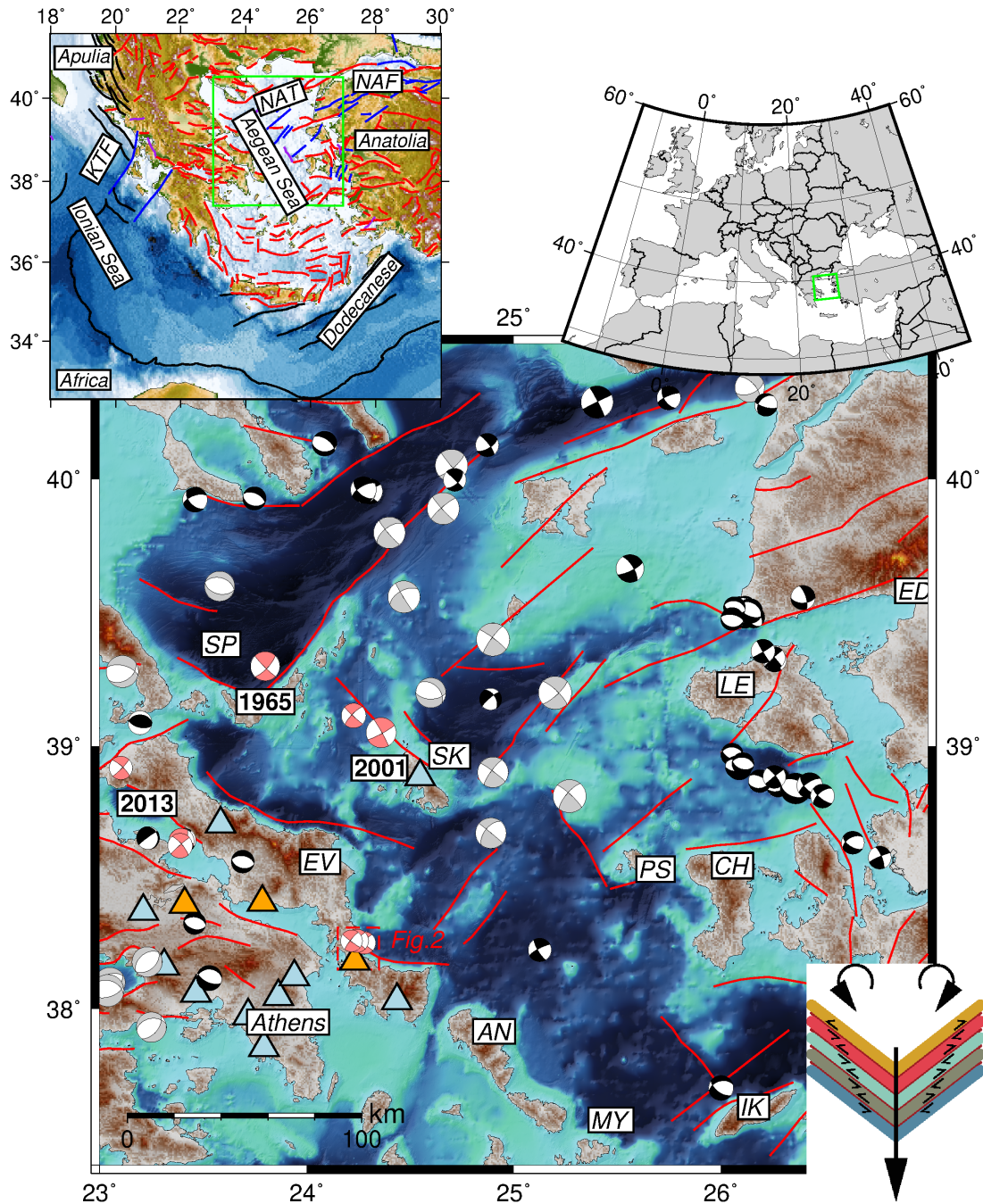
Figure 1 North and central Aegean map. NOA focal mechanisms for earthquakes greater than Mw 4.5 from 2012 onwards are plotted in black (Triantafyllis et al., 2021). Focal mechanisms for events greater than Mw 6 between 1967 and 2012 are plotted in gray, derived from the Centroid Moment Tensor (CMT) catalog (Dziewonski et al., 1981) and other local studies (Kiratzi et al., 1991; Taymaz et al., 1991; Konstantinou et al., 2010). The light red symbols show focal mechanisms obtained by this study and others (Roumelioti et al., 2003; Ganas et al., 2005; Kiratzi, 2014). Fault traces from the GEM Global Active Faults Database (Styron and Pagani, 2020) are plotted in red. Permanent stations used in this study from HL (National Observatory of Athens, Institute of Geodynamics, Athens, 1975) and HA (University of Athens, 2008) seismic networks are shown in blue triangles. Temporary stations from seismic network 1Y (Wolfgang Friederich et al., 2022) are shown in orange triangles. AN: Andros Island, CH: Chios island, ED: Edremit, EV: Evia island, IK: Ikaria island, LE: Lesvos island, MY: Mykonos basin, PS: Psara island, SK: Skyros basin, SP: Sporades basin. Top left inset map: A general map view of the Hellenic subduction zone where the African plate subducts beneath the Aegean area, bounded by the dextral North Anatolian Fault (NAF) and North Aegean Trough (NAT) in the northeast and the Kefalonia Transform Fault (KTF) in the west. Traces of normal, dextral strike-slip, sinistral strike-slip, and reverse faults from the GEM database are plotted in red, blue, purple, and black, respectively. The green box outline marks the north and central Aegean area shown in the main figure. Top right inset: A general map view of Europe. The green box outline is similar to the other inset. Lower right inset sketch: a graphical illustration based on Yaltırak et al. (2012) for the broken slat model proposed by Taymaz et al. (1991) depicts the transition from dextral strike-slip systems in the east to sinistral ones in the west.

rate of 50 m/day, ultimately leads up to the date of the two main events on November 29, 2022. Interestingly, a comparable migration speed of 70 m/day was identified during the Thiva 2020-2021 earthquake sequence, occurring just 80 km to the northwest. In that case, the migration was attributed to the diffusion of pore-fluid pressure on a normal fault (Kaviris et al., 2022). As the rupture zone transitions towards onshore regions in the northwest, there is a decrease in the number of relocated events. These remaining events that are observed in onshore regions tend to occur at greater depths, typically ranging from 10 to 12 km. A vertical cross-section perpendicular to the 130° strike images the existence of a fault zone oriented in a NW-SE direction with a steep SW dip (Fig. 2c). The MT of the largest event shows a fault dip that is parallel to the aftershock lineations observed on the eastern fault (Fig. S2). The clustered lineations observed in Figures 2 and S2 indicate the presence of another fault running parallel to the west.

A noticeable cluster of seismic activity is observed in the northwest region, near Zarakes village, which is distinct from the main rupture zone (Fig. 2). This particular cluster is separated from the main rupture zone by a higher topographic relief zone that spans approximately 3 km in length. The abundance of seismic activity in this elevated area suggests two possible scenarios. Firstly, there could be a separate secondary fault within the NW-SE strike-slip fault zone. Alternatively, it could indicate a larger fault zone that fractures into segments, with an unbroken section in the middle.

The analysis of the relocated catalog reveals the presence of numerous offshore events that exhibit a general SW-NE direction. However, due to the limited availability of seismic stations in the eastern offshore region, most of the eastward events have not been relocated using WCC techniques. As a result, SW-NE alignments are not as clearly defined in the relocated catalog. If some SW-NE lineations were more clearly evident, they could potentially be associated with the dextral strike observed in most calculated MTs, which is approximately 220°. However, based on the available MTs and the WCC relocations, there is no conclusive evidence of any significant event occurring along a right-lateral offshore fault (Fig. 2). Therefore, the relocation of this earthquake sequence suggests an asymmetric rupture taking place within a steep NW-SE fault zone, which persists for at least 6 months. It also emphasizes the need for better coverage of seismic stations to overcome this limitation and obtain a more complete picture of the seismic activity, particularly in offshore regions in the Aegean. This consideration is crucial for improving our understanding of fault structures and earthquake mechanisms in the study area.

As the Hellenic subduction zone is rolling back towards the southwest, a pair of opposite rotations occur. Dextrally rotated blocks are observed between the Kefalonia Transform Fault (KTF) and the western edge of the Aegean Sea across Skyros, Evia, etc (Fig. 1). Conversely, on the other side of the Aegean, the southeast Dodecanese islands, Crete, and southwestern Turkey blocks undergo sinistral rotation (e.g. Martin, 2007). In the middle, the Aegean microplate is constrained by two

rigid indentors, the Anatolia (eastern end) and the Apulia (western end) platforms (e.g. Wallace et al., 2009). The proposed model, referred to as the "dual indentor" model, describes the opposing rotation of mainland Greece in a dextral-clockwise direction and Anatolia in a sinistral-anticlockwise direction. This concept bears resemblance to the pinned, broken slat model introduced Taymaz et al. (1991), as well as the "double saloon door" concept put forth by Martin (2007). Considering that the kinematics of the northern and central Aegean can be described from the broken slat model of Taymaz et al. (1991), where a right-hand margin of parallel slats has rotated more than the left, there are points of abrupt change in slip vector, the breakpoints on the slats, that produce conjugate strike-slip fault structures (Fig. 1). Distinct conjugate areas can be identified from north to south based on focal mechanisms. These structures may not exhibit similar seismic activity in terms of temporal occurrence and density. Instead, they serve as indicators of the transition from predominantly dextral to sinistral strike-slip motions. Such areas include the region between Skopelos and Alonissos islands in the Sporades basin, marking the termination of the Northern Aegean Trough (Fig. 1). Another area is found near the Skyros basin, signifying the end of the Skyros-Edremit Trough. Additionally, the South Evia area, the region focused on in this study, lies at the termination of another branch of the Lesvos-Edremit fault system (Fig. 1). Further south, the extension of the Chios-Psara fault system suggests a potential conjugate fault structure between Evia and Andros islands (Fig. 1). Additionally, if the extension of the Ikaria faults, which currently lacks any recorded MTs, exhibits a similar sense of motion, it could potentially indicate the presence of a similar geological structure within the Mykonos basin (Fig. 1).

The existence of these fault structures in the western Aegean that marks the transition from SW-NE dextral strike-slip ruptures to NW-SE sinistral strike-slip ruptures links the Aegean shear zone with the normal faulting in the mainland (Kiratzi, 2014). The first well-documented occurrence of left-lateral strike-slip motions can be traced back to the 2001 Skyros earthquake (Roumelioti et al., 2003; Ganas et al., 2005). Several preceding significant earthquakes, such as the 1965 event in the Sporades basin (Fig. 1), may be also associated with left-lateral strike-slip motions (Kiratzi, 2014). Furthermore, a small seismic sequence on the western shores of northern Evia, which occurred in November 2013, offered supplementary evidence for left-lateral strike-slip motions (Kiratzi, 2014).

The South Evia 2022-2023 sequence has emerged as the southernmost observed area where strike-slip NW-SE faults have been activated. This finding contradicts previous assumptions regarding the relatively low seismicity in the region east of the Athens metropolis. It also implies the potential activation in the future of similar zones, either between Evia and Andros islands or even between Tinos and Mykonos islands in the south (Fig. 1). Consequently, seismic hazard maps for the area need to be reassessed to incorporate this new information and ensure precise evaluations of seismic risk.
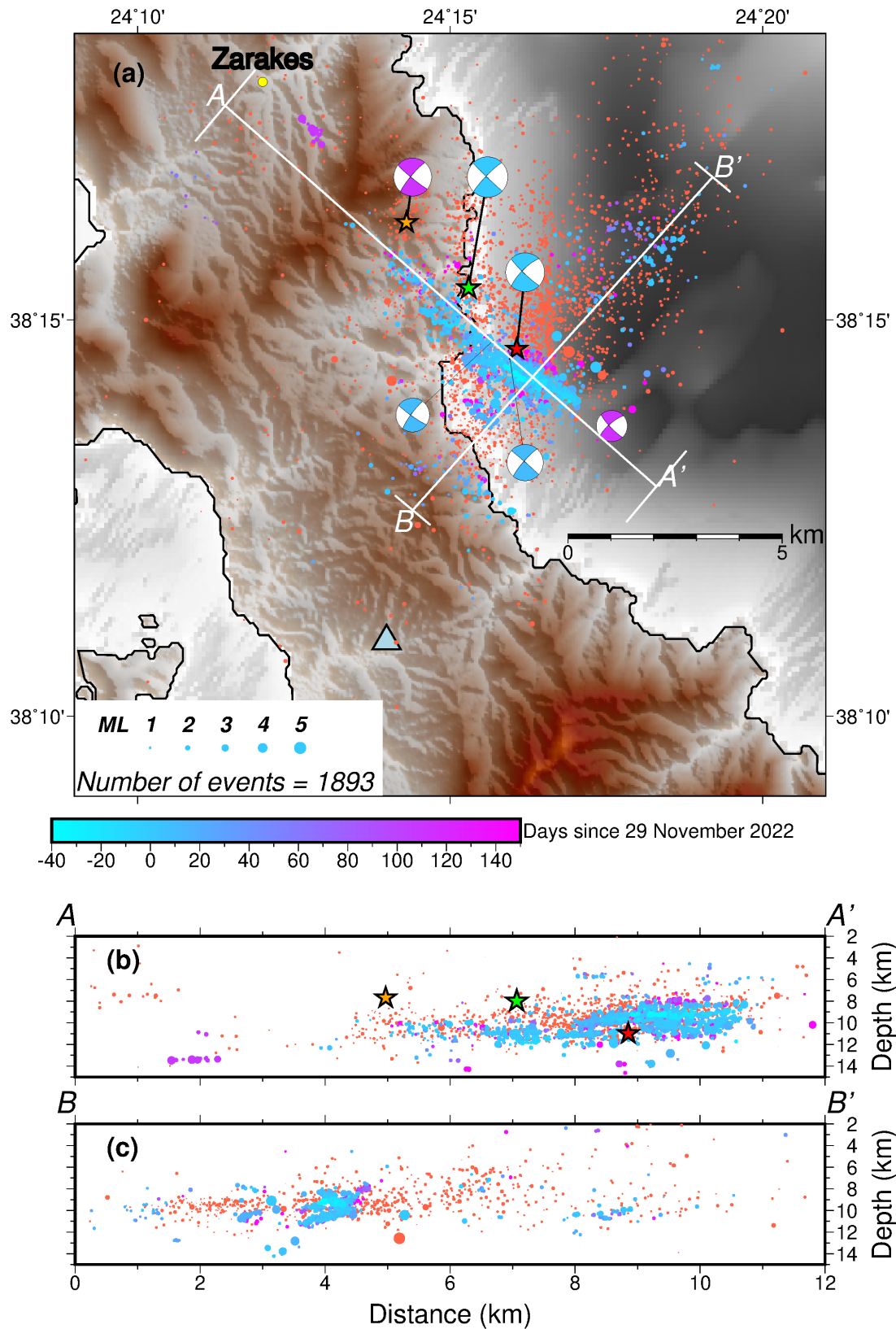
Figure 2 (a) Relocated 2022-2023 earthquake sequence colored based on days since November 29th, 2022, sized proportionally to their local magnitude. Hypocenters in light red are those detected events not relocated with WCC. Moment tensor solutions are colored similarly to the hypocenters. Red and green stars indicate the location of the two largest events of the sequence on the 29th of November 2022. The orange star marks the Mw 4.5 aftershock on April 22, 2023 (b) NW-SE vertical cross-section along fault strike. (c) SW-NE vertical cross-section with orthogonal orientation to the strike of the main fault. The width of the cross-sections are 2 km and 1 km, respectively. Hypocenter colors in vertical cross-sections are similar to the map view in (a).
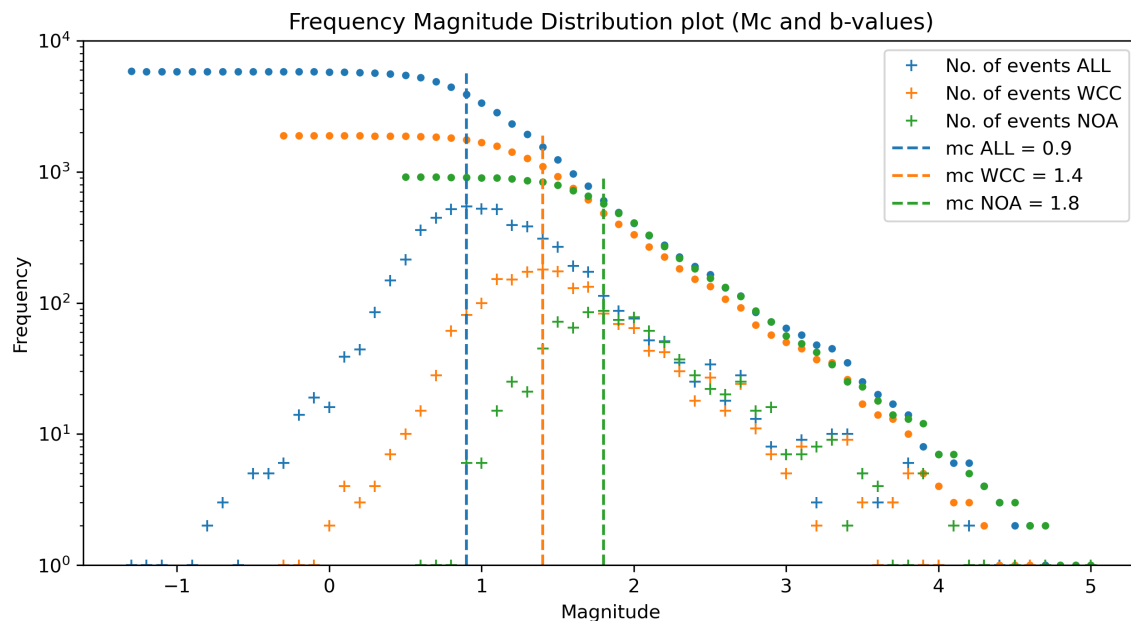
Figure 3 The Frequency-Magnitude distribution (FMD) of the detected (ALL), relocated (WCC), and NOA catalogs with a bin width of 0.1. Colored crosses and circles show the number and the cumulative number of events per magnitude bin, respectively. The magnitudes of completeness (Mc) are estimated using the Maximum Curvature method proposed by Wiemer and Wyss (2000).

Acknowledgements

Data and code availability

The relocated catalog is available in Zenodo data repository (Evangelidis and Fountoulakis, 2023). Broadband seismic records, acquired from the HL (National Observatory of Athens, Institute of Geodynamics, Athens, 1975), HA (University of Athens, 2008), HP University of Patras (2000), and 1Y (Wolfgang Friederich et al., 2022) networks were accessed through the National Observatory of Athens data center node (EIDA@NOA, http://eida.gein.noa.gr) (Evangelidis et al., 2021). Routine seismic catalog locations have been obtained from NOA FDSN event webservice http://eida.gein.noa.gr/fdsnws/event/1/ and MTs are available at https://bbnet.gein.noa.gr/HL/seismicity/mts. For further information regarding the AdriaArray initiative visit https://orfeus.readthedocs.io/en/latest/adria_array_main.html. Bathymetry has been downloaded from EMODnet portal http://portal.emodnet-bathymetry.eu/gebco-bathymetry-basemap and GEBCO (GEBCO Compilation Group, 2023). The land topography data used in this study was obtained from the NASA Shuttle Radar Topography Mission Global dataset, which has a resolution of 1 arc second (NASA JPL, 2013).

Competing interests

References

Barbot, S. and Weiss, J. R. Connecting subduction, extension and shear localization across the Aegean Sea and Anatolia. *Geophysical Journal International*, 226(1):422–445, 02 2021. doi: 10.1093/gji/ggab078.

Beyreuther, M., Barsch, R., Krischer, L., Megies, T., Behr, Y., and Wassermann, J. ObsPy: A Python Toolbox for Seismology. *Seismological Research Letters*, 81(3):530–533, 05 2010. doi: 10.1785/gssrl.81.3.530.

Caputo, R. and Pavlides, S. The Greek Database of Seismogenic Sources (GreDaSS), version 2.0.0: A compilation of potential seismogenic sources (Mw > 5.5) in the Aegean Region. *GreDaSS*, 2013. doi: 10.15160/unife/gredass/0200.

Danciu, L., Nandan, S., Reyes, C., Basili, R., Weatherill, G., Beauval, C., Rovida, A., Vilanova, S., Sesetyan, K., Bard, P.-Y., Cotton, F., Wiemer, S., and Giardini, D. The 2020 update of the European Seismic Hazard Model: Model Overview. *European Facilities for Earthquake Hazard and Risk, EFEHR Technical Report 001, v1.0.0*, 2021. doi: 10.12686/a15.

Dziewonski, A. M., Chou, T.-A., and Woodhouse, J. H. Determination of earthquake source parameters from waveform data for studies of global and regional seismicity. *Journal of Geophysical Research: Solid Earth*, 86(B4):2825–2852, 1981. doi: 10.1029/JB086iB04p02825.

Evangelidis, C. P. and Fountoulakis, I. Supplementary Dataset for the Report "Imaging the Western Edge of the Aegean Shear Zone: The South Evia 2022-2023 Seismic Sequence". 2023. doi: 10.5281/zenodo.8077688.

Evangelidis, C. P., Triantafyllis, N., Samios, M., Boukouras, K., Kontakos, K., Ktenidou, O., Fountoulakis, I., Kalogeras, I., Melis,

N. S., Galanis, O., Papazachos, C. B., Hatzidimitriou, P., Scordilis, E., Sokos, E., Paraskevopoulos, P., Serpetsidaki, A., Kaviris, G., Kapetanidis, V., Papadimitriou, P., Voulgaris, N., Kassaras, I., Chatzopoulos, G., Makris, I., Vallianatos, F., Kostantinidou, K., Papaioannou, C., Theodoulidis, N., Margaris, B., Pilidou, S., Dimitriadis, I., Iosif, P., Manakou, M., Roumelioti, Z., Pitilakis, K., Riga, E., Drakatos, G., Kiratzi, A., and Tselentis, G. Seismic Waveform Data from Greece and Cyprus: Integration, Archival, and Open Access. *Seismol. Res. Lett.*, 92(3):1672–1684, 2021. doi: 10.1785/0220200408.

Fountoulakis, I., Evangelidis, C. P., and Ktenidou, O. Coseismic and Postseismic Imaging of a Composite Fault System: The Samos 2020 Mw 7.0 Sequence. *Bull. Seismol. Soc. Am.*, 03 2023. doi: 10.1785/0120220207.

Ganas, A., Drakatos, G., Pavlides, S., Stavrakakis, G., Ziazia, M., Sokos, E., and Karastathis, V. The 2001 Mw = 6.4 Skyros earthquake, conjugate strike-slip faulting and spatial variation in stress within the central Aegean Sea. *Journal of Geodynamics*, 39(1):61–77, 2005. doi: 10.1016/j.jog.2004.09.001.

Ganas, A., Oikonomou, I. A., and Tsimi, C. NOAfaults: a digital database for active faults in Greece. *Bulletin of the Geological Society of Greece*, 47(2):518–530, Jan. 2013. doi: 10.12681/bgsg.11079.

GEBCO Compilation Group. GEBCO 2023 Grid. *GEBCO 2023 Grid. British Oceanographic Data Centre, National Oceanography Centre, UK*, 2023. doi: 10.5285/f98b053b-0cbc-6c23-e053-6c86abc0af7b.

Kaviris, G., Kapetanidis, V., Spingos, I., Sakellariou, N., Karakonstantis, A., Kouskouna, V., Elias, P., Karavias, A., Sakkas, V., Gatsios, T., Kassaras, I., Alexopoulos, J. D., Papadimitriou, P., Voulgaris, N., and Parcharidis, I. Investigation of the Thiva 2020 - 2021 Earthquake Sequence Using Seismological Data and Space Techniques. *Applied Sciences*, 12(5), 2022. doi: 10.3390/app12052630.

Kiratzi, A., Wagner, G., and Langston, C. Source parameters of some large earthquakes in Northern Aegean determined by body waveform inversion. *Pure and Applied Geophysics*, 135: 515–527, 1991. doi: 10.1007/BF01772403.

Kiratzi, A. A. *Mechanisms of Earthquakes in Aegean*, pages 1–22. Springer Berlin Heidelberg, Berlin, Heidelberg, 2014. doi: $10.1007/978-3-642-36197-5_299-1$.

Klein, F. W. User's guide to HYPOINVERSE-2000: A Fortran program to solve for earthquake locations and magnitudes. *U.S. Geol. Surv. Open-File Rept.*, page 02-171, 2002. doi: 10.3133/ofr02171.

Konstantinou, K. I., Melis, N. S., and Boukouras, K. Routine Regional Moment Tensor Inversion for Earthquakes in the Greek Region: The National Observatory of Athens (NOA) Database (2001–2006). *Seismological Research Letters*, 81(5):750–760, 09 2010. doi: 10.1785/gssrl.81.5.750.

Konstantinou, K. I., Mouslopoulou, V., and Saltogianni, V. Seismicity and Active Faulting around the Metropolitan Area of Athens, Greece. *Bull. Seismol. Soc. Am.*, 110(4):1924–1941, 06 2020. doi: 10.1785/0120200039.

Lomax, A., Virieux, J., Volant, P., and Berge, C. Probabilistic earthquake location in 3D and layered models: Introduction of a Metropolis-Gibbs method and comparison with linear locations. In Thurber, C. H. and Rabinowitz, N., editors, *Advances in Seismic Event Location*, pages 101–134. Kluwer, Amsterdam, 2000. doi: $10.1007/978-94-015-9536-0_5$.

Martin, A. Gondwana breakup via double-saloon-door rifting and seafloor spreading in a backarc basin during subduction rollback. *Tectonophysics*, 445(3):245–272, 2007. doi: 10.1016/j.tecto.2007.08.011.

Mousavi, M. S., Ellsworth, W. L., Zhu, W., Chuang, L. Y., and Beroza, G. C. Earthquake transformer—an attentive deep-learning model for simultaneous earthquake detection and phase picking. *Nature Communications*, 11:3952, 2020. doi: 10.1038/s41467-020-17591-w.

NASA JPL. NASA Shuttle Radar Topography Mission Global 1 arc second. *Distributed by NASA EOSDIS Land Processes DAAC*, 2013. doi: 10.5067/MEaSUREs/SRTM/SRTMGL1.003.

National Observatory of Athens, Institute of Geodynamics, Athens. National Observatory of Athens Seismic Network. *International Federation of Digital Seismograph Networks*, 1975. doi: 10.7914/SN/HL.

Roumelioti, Z., Kiratzi, A., and Melis, N. Relocation of the 26 July 2001 Skyros Island (Greece) earthquake sequence using the double-difference technique. *Physics of the Earth and Planetary Interiors*, 138(3):231–239, 2003. doi: 10.1016/S0031-9201(03)00138-9.

Scordilis, E. M., Kementzetzidou, D., and Papazachos, B. C. Local magnitude calibration of the Hellenic Unified Seismic Network. *Journal of Seismology*, 20(1):319–332, 2016. doi: 10.1007/s10950-015-9529-5.

Styron, R. and Pagani, M. The GEM Global Active Faults Database. *Earthquake Spectra*, 36(1_suppl):160–180, 2020. doi: 10.1177/8755293020944182.

Taymaz, T., Jackson, J., and McKenzie, D. Active tectonics of the north and central Aegean Sea. *Geophysical Journal International*, 106(2):433–490, 1991. doi: 10.1111/j.1365-246X.1991.tb03906.x.

Triantafyllis, N., Venetis, I. E., Fountoulakis, I., Pikoulis, E., Sokos, E., and Evangelidis, C. P. Gisola: A High-Performance Computing Application for Real-Time Moment Tensor Inversion. *Seismological Research Letters*, 2021. doi: 10.1785/0220210153.

Trugman, D. T. and Shearer, P. M. GrowClust: A Hierarchical Clustering Algorithm for Relative Earthquake Relocation, with Application to the Spanish Springs and Sheldon, Nevada, Earthquake Sequences. *Seismological Research Letters*, 88(2A):379–391, 2017. doi: 10.1785/0220160188.

University of Athens. Hellenic Seismological Network, University of Athens, Seismological Laboratory. *International Federation of Digital Seismograph Networks*, 2008. doi: 10.7914/SN/HA.

University of Patras. University of Patras, Seismological Laboratory. *International Federation of Digital Seismograph Networks*, 2000. doi: 10.7914/SN/HP.

Wallace, L. M., Ellis, S., and Mann, P. Collisional model for rapid fore-arc block rotations, arc curvature, and episodic back-arc rifting in subduction settings. *Geochemistry, Geophysics, Geosystems*, 10(5), 2009. doi: 10.1029/2008GC002220.

Wessel, P. and Smith, W. H. New, improved version of Generic Mapping Tools released. *Eos, Transactions American Geophysical Union*, 79(47):579–579, 1998. doi: 10.1029/98EO00426.

Wiemer, S. and Wyss, M. Minimum Magnitude of Completeness in Earthquake Catalogs: Examples from Alaska, the Western United States, and Japan. *Bulletin of the Seismological Society of America*, 90(4):859–869, 08 2000. doi: 10.1785/0119990114.

Wolfgang Friederich, Christos Evangelidis, Costas Papazachos, Efthimios Sokos, George Kaviris, and Dragana Cernih. AdriaArray Temporary Network: Greece, North Macedonia. *International Federation of Digital Seismograph Networks*, 2022. doi: 10.7914/y0t2-3b67.

Yaltırak, C., İşler, E., Aksu, A., and Hiscott, R. Evolution of the Bababurnu Basin and shelf of the Biga Peninsula: Western extension of the middle strand of the North Anatolian Fault Zone, Northeast Aegean Sea, Turkey. *Journal of Asian Earth Sciences*, 57:103–119, 2012. doi: 10.1016/j.jseaes.2012.06.016.

Zhang, M., Ellsworth, W. L., and Beroza, G. C. Rapid Earthquake
 Association and Location. *Seismological Research Letters*, 90(6):
 2276–2284, 2019. doi: 10.1785/0220190052.